Hindawi
International Journal of Spectroscopy
Volume 2018, Article ID 7160381, 15 pages
https://doi.org/10.1155/2018/7160381

Research Article

Application of Electrochemical Techniques on Study of Effect of Nano-ZnO in Conductive Polyaniline Containing Zinc-Rich Primer

Ximing Li[1] **and Homero Castaneda**[2]

[1]*Chemical and Biomolecular Engineering, The University of Akron, Akron, OH 44325, USA*
[2]*Materials Science and Engineering, Texas A&M University, College Station, TX 77843, USA*

Correspondence should be addressed to Ximing Li; xmli2012@gmail.com

Received 31 August 2017; Revised 20 December 2017; Accepted 10 January 2018; Published 28 February 2018

Academic Editor: Stefan Schmatz

Effect of zinc oxide nanoparticles on anticorrosion performance has been studied in conductive polyaniline containing zinc-rich primer in 3.5 wt% NaCl solution, using Electrochemical Impedance Spectroscopy (EIS) and localized electrochemical Scanning Vibrating Electrode Technique (SVET). The results showed that the addition of nano-zinc oxide particles in conductive polyaniline containing zinc-rich primer made the reaction of zinc more stable and slower, further increasing the effective cathodic protection period. EIS and SVET results confirmed that three performance evolution stages were obtained for zinc-rich primer being immersed in 3.5 wt% sodium chloride solution.

1. Introduction

Zinc-rich epoxy primer (ZRP) has been used as anticorrosion primers since the 1930s [1, 2], highly recommended for offshore environments, refineries, power plants, bridges, and so forth. ZRPs are expected to provide sacrificial cathodic protection (CP) at an early stage, and the formation of zinc oxide products would provide further barrier protection at later stage [3]. Intrinsically conductive pigment has been added in ZRP to improve CP efficiency, of which polyaniline (PAni) was studied due to its excellent environmental stability, controllable electrical conductivity, and interesting redox properties [4–7]. In our previous work [8], different PAni states including nonconductive emeraldine base (EB) and conductive emeraldine salt (ES) were added to ZRP, to study the effects of different oxidation states on anticorrosive performance. EB is electrically neutral while doped (protonated), and the resulting ES form is highly electrically conductive. The addition of a small amount of conductive PAni to ZRP slowed the activation process of zinc particles and further improved the cathodic protection effect, while the nonconductive PAni EB accelerated the activation of zinc particles. The formed zinc oxide products were compact and provided better barrier performance than the commercial ZRP.

Coatings combined with metal oxide nanoparticles such as ZnO [9], TiO_2 [10], and Fe_2O_3 [11] would provide better corrosion resistance and improved protection when combined with PAni. This is because the combination of nano-metal oxide powders and coating matrix tends to produce crack-free, uniform coating interface and also helps to form uniform passive layers on the surface of metallic substrate. Mostafaei and Nasirpouri [9] synthesized a series of conducting PAni-ZnO nanocomposites materials, and the study results showed that the addition of ZnO nanorods and PAni significantly improved the barrier and corrosion protection performance of the epoxy coating. The increased inhibition of PAni in the presence of metal cations like Zn^{2+} ions would likely be attributed to the formation of compact clusters and enhanced by more amounts of electron rich benzenoid groups that facilitates the greater adsorption on the iron surface and hereby prevents further corrosion

[12]. Furthermore, ZnO nanostructured materials may act as barrier in the paint film and may reduce passing routes used by electrolyte and corrosive ions. The studies of protection performance of combination of PAni with ZRP are still limited [13]. More studies are needed on the application of PAni on ZRP to obtain a more protective coating that will combine both PAni and ZRP properties.

To investigate the anticorrosion performances of metal rich coatings, Electrochemical Impedance Spectroscopy (EIS) has been considered as a common technique to characterize and quantify the performance of typical coatings exposed to a corrosive environment [14–17]. EIS provides qualitative and quantitative magnitudes that characterize the performance of the coating under exposed conditions [18–21]. Different processing methods and fitting models were designed, to investigate the corrosion protective mechanisms [22–26]. Although EIS is a valuable technique for studying dielectric properties, it fails to provide enough spatial resolution and only an average behavior can be achieved on the studied surface. The idea of a localized measurement is to examine areas within a sample that differ in their activity individually, which has promoted many studies. Recently, the development of microelectrode techniques and scanning electrode techniques has made it possible to measure electrochemical processes on a local scale, which has attracted lots of studied on the local electrochemical processes on corroding surfaces and investigations of localized corrosion [27]. Scanning Vibrating Electrode Technique (SVET) is a powerful tool to permit a better understanding of the mechanisms and processes of corrosion at defects and underneath coatings [28]. This technique can provide valuable information of the electrochemical interactions between a coating and its substrate at a defect. The analysis of the current distribution would be useful considering the anticorrosion mechanism including the generation and development of defects and the influence of pigments/inhibitors on corrosion of substrate at a defect.

This work is to investigate the performance of PAni-nano-ZnO containing ZRPs in a 3.5 wt% NaCl environment and characterize the associated mechanisms. Different electrochemical microscopy techniques were used in this work, including electrochemical and localized scanning vibrating electrode spectroscopy technique.

2. Experimental Design

2.1. Materials and Preparation. The 1008 steel samples were used in this work. All the samples were mechanically grinded with different grit sizes of SiC papers to 1200, used as substrate coated with the developed paint. Before application, they were degreased with acetone and ethanol solution in an ultrasonic bath to remove the impurities and rinsed thoroughly with double distilled water and dried in the air.

PAni emeraldine base (PAni EB), molecular weight ca. 65,000, was supplied by the Aldrich Chemical Company. All the other chemicals were obtained from Aldrich in analytical grade purity. Conductive PAni emeraldine salt (PAni ES) was prepared by dispersing 10 g PAni EB in 250 ml of 1 mol·dm−3 ethanolic solution of phenylphosphonic acid and stirring overnight. Then the PAni ES product was filtered, washed with distilled water, air-dried, and subsequently ground under liquid nitrogen to give powders of <20 μm particle size.

Zinc-rich primer used in this work (Amercoat® 68HS) is a commercial polyamide cured epoxy resin pigmented with zinc dust pigment, purchased from PPG industries. It is composed of epoxy base, hardener, and zinc dust, which contains approximately 80% zinc in dry film with 70% ± 3% volume solids. Zinc oxide, nanoparticles (<130 nm), 40 wt.% dispersed in ethanol, was purchased from Aldrich Chemical Company, whose density is 1.25 g/ml ± 0.05 g/ml at 25°C. Two paints are designed: PAni-ZRP and PAni-ZnO-ZRP. For PAni-ZRP paint, conductive PAni powder synthesized above was added in the premixed ZRP coating component by 0.2 wt.% under agitation until fully mixed. For PAni-ZnO-ZRP paint, 0.1 wt.% PAni powder and 0.3 wt% nano-zinc oxide powders were added accordingly to the premixed ZRP system under agitation until fully mixed. Coatings were then painted by high pressure spraying on prepared panels. The average dry coating thickness was detected, in the range of 170–180 um.

2.2. Testing Environments and Methods

2.2.1. Coating Characterization and Weight Loss Test. After the prepared samples were completely dry, contact angle test was applied to check the tendency of water uptake on the coating surface according to ASTM D7334 [29]. Four-pin conductivity tester was applied to check the percolation condition of various coating systems. Weight loss test was designed to check the cathodic reaction of zinc particles and formation of zinc oxide products in coating interface. The coated samples (in duplicate) were taped at the back side and edges, leaving the tested area of 1 cm × 1 cm, and then were immersed in 3.5 wt% NaCl solution over a period of 120 days at room temperature. Before and after being immersed, all the samples were weighted, to check the weight loss conditions. The surface morphology of the specimens was observed by Field Emission Scanning Electron Microscope (SEM) at a beam energy of 5 keV, accompanied by energy-dispersive X-ray spectroscopy (EDS). In addition, pH of the electrolyte was monitored from time to time.

2.2.2. Electrochemical Spectroscopy Technique Measurements. The EIS tests were conducted using Gamry Reference 600™ Potentiostat instrument. Three-electrode system was applied for electrochemical tests: steel samples serving as working electrode, saturated calomel electrode (SCE) as the reference electrode, and platinum mesh as counterelectrode. In EIS, an alternating current signal with a frequency range from 100 kHz to 10 mHz and amplitude of 10 mV was applied to the working electrode at the corrosion potential. Besides, open circuit potential (OCP) was also recorded in each study system, to check the electrochemical status. All the tests are set at room temperature over a period of 120 days, in 3.5 wt% NaCl to simulate chloride neutral corrosive environment. Duplicate samples are considered for each test to verify the repeatability.

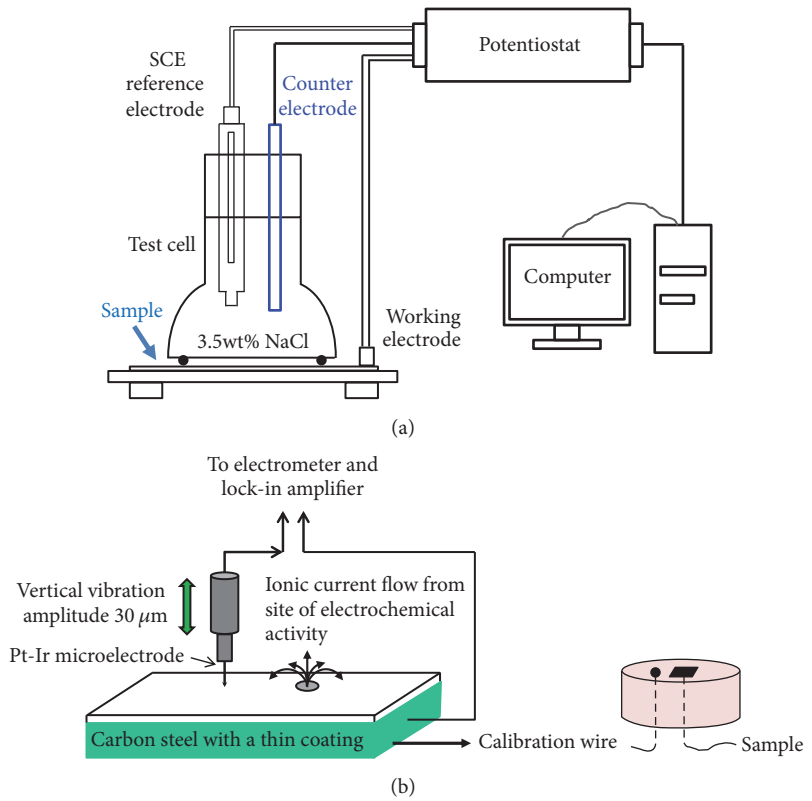

Figure 1: Illustration diagram of EIS test system (a) and SVET Scanning System (b).

SVET was tested by VersaScan™ Electrochemical Scanning System. The SVET microelectrode applied was a Pt–Ir microelectrode (Microprobe Inc.) with a 10 μm diameter tip. The vibrating separation of the microprobe was around 100 μm above the samples with the amplitude 20 μm along the X and Y directions. A platinum wire circle was used as the reference and counterelectrodes when performing the calibration process. The ZRP samples ($1 \times 1\,cm^2$) were protected by a polyester tape to make the exposed area of $3 \times 3\,mm^2$ to be the scanning area. An artificial scratch was introduced to half of the scanning area, to simulate the galvanic couple of ZRPs and steel substrate. The probe would move across with a 31×31 scan, generating a 961-point mesh across the surface. Scans were initiated 10 s after immersion and repeated every half an hour. All of the SVET measurements were performed in duplicate at OCP in 0.01 wt% NaCl solution. The experimental setup for these two electrochemical tests are shown in Figure 1.

3. Results and Discussion

3.1. Coating Characterization and Weight Loss Test. The test result of coating surface hydrophobicity is shown in Figure 2. PAni-ZRP and PAni-ZnO-ZRP exhibited a much larger contact angle value than the commercial ZRP, which indicates both two coatings are more hydrophobic than zinc-rich primer coating. This property would postpone the activation time of zinc particles after being immersed in sodium chloride solution, in agreement with the previous study [8]. Comparing these two coatings, the addition of zinc oxide nanoparticles does not change the coating surface hydrophobic property so much, just a little bit of ignorable increase. It makes sense that the surface property of zinc oxide particle is similar to zinc particle (spontaneous oxides on the surface). The main factor would be conductive polyaniline, making the surface more hydrophobic. The resistivity ρ holds an opposite relationship with conductivity, which can indicate the Zn-to-Zn connection condition of ZRPs. The small amount of conductive PAni improved the Zm-to-Zn condition of the ZRP, which has been discussed in previous study [8], while the addition of nano-ZnO particles in PAni-ZRP increased the dry coating resistivity with large derivation, probably because of the addition of ZnO and the combination of ZnO and PAni which counteract the effect of conductive polyaniline in ZRP.

The results of solution pH and sample weight loss were plotted in Figure 3, for PAni-ZRP with and without ZnO nanoparticles. The pH for 3.5 wt% NaCl solution is 6.39. The pH evolution of these two systems is similar over time: a quick increase during the first 5 d followed by a slow increase till 120 d. The increase of pH is due to the cathodic reaction listed in the following:

$$\frac{1}{2}O_2 + H_2O + 2e^- \longrightarrow 2OH^- \quad (1)$$

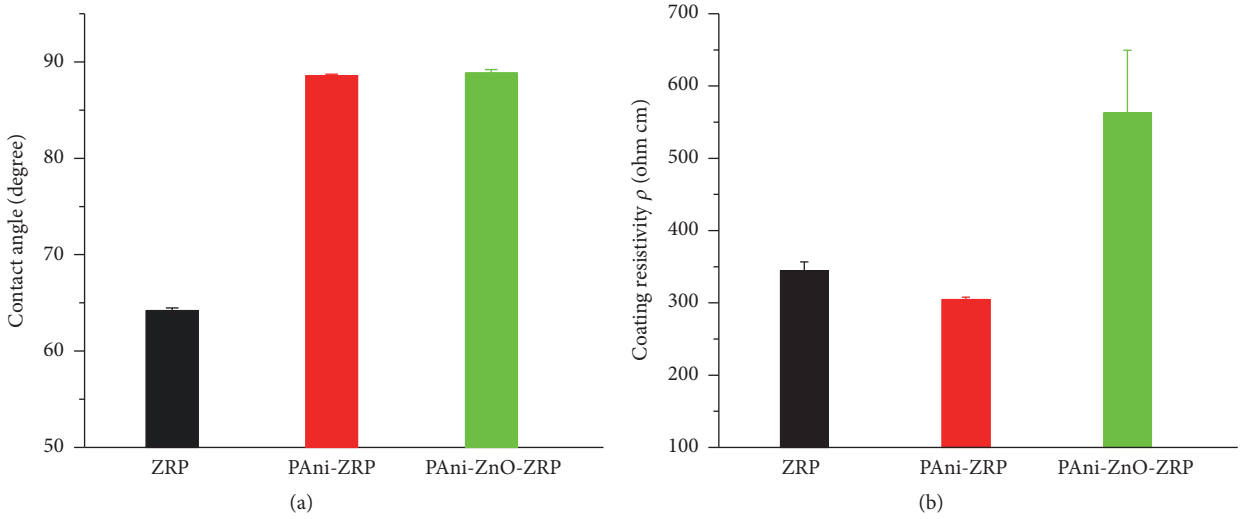

Figure 2: Contact angle (a) and coating resistivity ρ (b) of PAni-ZRP and PAni-ZnO-ZRP.

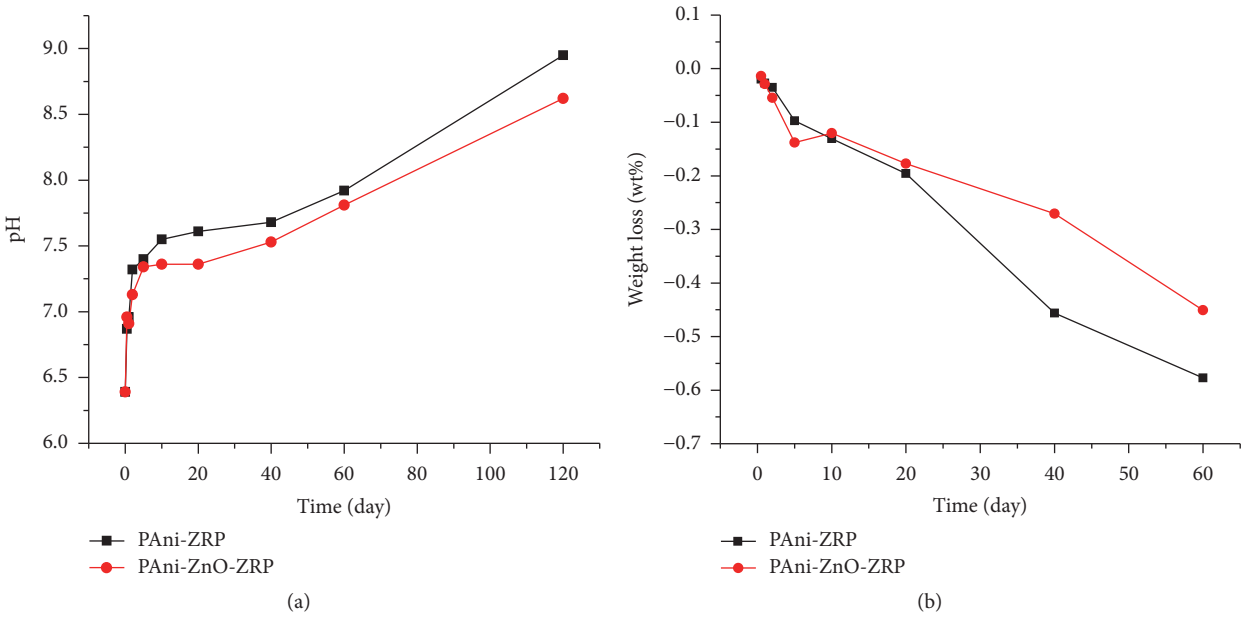

Figure 3: Solution pH and weight loss of sample PAni-ZRP and PAni-ZRP-ZnO over time.

Later, due to alkaline environment, the corrosion of Zn may be related to the following equations. This makes the second period exhibit a slowly increasing pH.

$$Zn^{2+} + H_2O \longrightarrow ZnO + 2H^+ \quad (2)$$

$$5ZnO + 2Cl^- + 5H_2O \longrightarrow Zn_5(OH)_8Cl_2 + 2OH^- \quad (3)$$

The weight loss was negative meaning the formed zinc oxide products were compact and adhesive in the coating matrix. pH value of coating PAni-ZRP is larger than PAni-ZnO-ZRP, indicating the more reaction of zinc particles. In addition, this agrees with the weight loss data: PAni-ZRP gains more weight than PAni-ZnO-ZRP. Hence the addition of nano-ZnO in PAni-ZRP presents a slower zinc cathodic activation.

The surface morphologies of PAni-ZRP and PAni-ZnO-ZRP before test and after 60 d of immersion are shown in Figures 4 and 5, respectively. The surface morphology of coating PAni-ZnO-ZRP is more uniform and has less pores than PAni-ZRP (Figure 4). And after 60 d of immersion, the coating surface was covered by zinc oxide products; the oxide products of PAni-ZnO-ZRP are more compact. The cross-sectional SEM images after 60 d and 120 d are shown in Figure 6. Zinc particles at the inner coating matrix were also

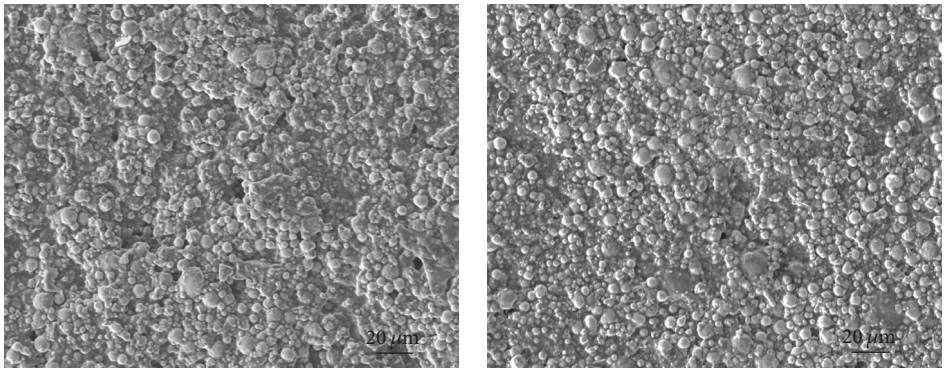

(a) (b)

Figure 4: Surface morphologies of PAni-ZRP (a) and PAni-nano-ZnO-ZRP (b) before test.

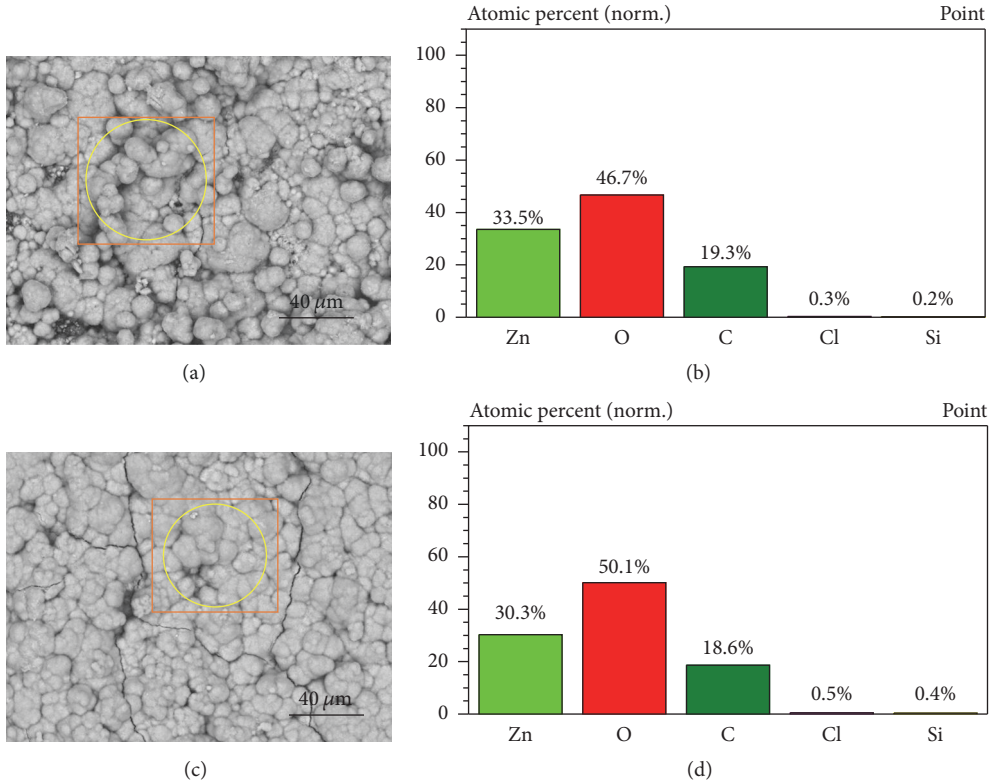

Figure 5: Surface morphologies of PAni-ZRP (a & b) and PAni-nano-ZnO-ZRP (c & d) after 60 d.

reacted for PAni-ZRP after 60 d of immersion (Figure 6(a)). The zinc oxide layer formed on PAni-ZnO-ZRP coating is more compact than PAni-ZRP, comparing Figure 5(a) and 5(c). And the EDS mapping was conducted at the coating matrix by scanning an area of 40 μm × 40 μm (above the steel substrate). Notably, even before test, the oxygen content was approximately 10 wt% at the zinc particle surface because of the presence of native zinc oxide. The EDS mappings of element of Zn, O, Cl, and Fe were detected to track the water/ions transportation and cathodic reaction of zinc particles in coating/steel interface (Figure 7). Before 20 d, the mass percent of element O and Cl in coating PAni-ZRP is higher than PAni-ZnO-ZRP, indicating that water and ions transported to the coating PAni-ZRP interface quicker than PAni-ZnO-ZRP. This shows that the addition of nano-zinc oxide may reduce the passing routes of water/ions and improves the coating barrier performance, in agreement with published literature [30]. In addition, a small amount of iron was detected for PAni-ZRP at 120 d, showing an localized attack of substrate corrosion.

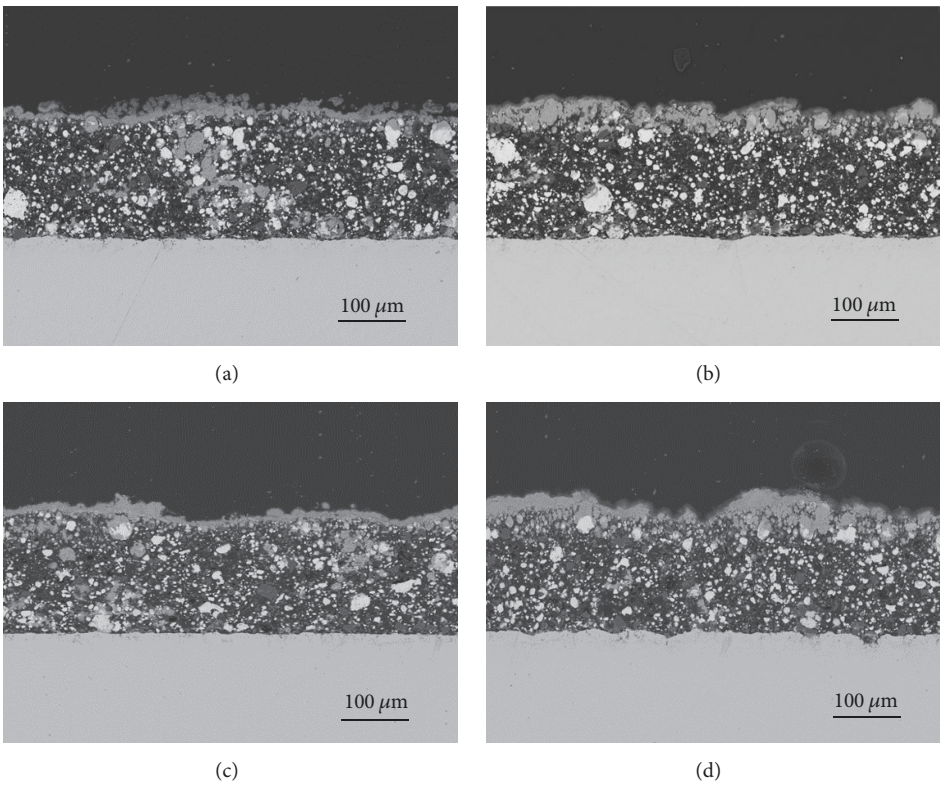

Figure 6: Cross-sectional morphologies of PAni-ZRP (a & b) and PAni-nano-ZnO-ZRP (c & d) after 60 days (a & c) and 120 days (b & d).

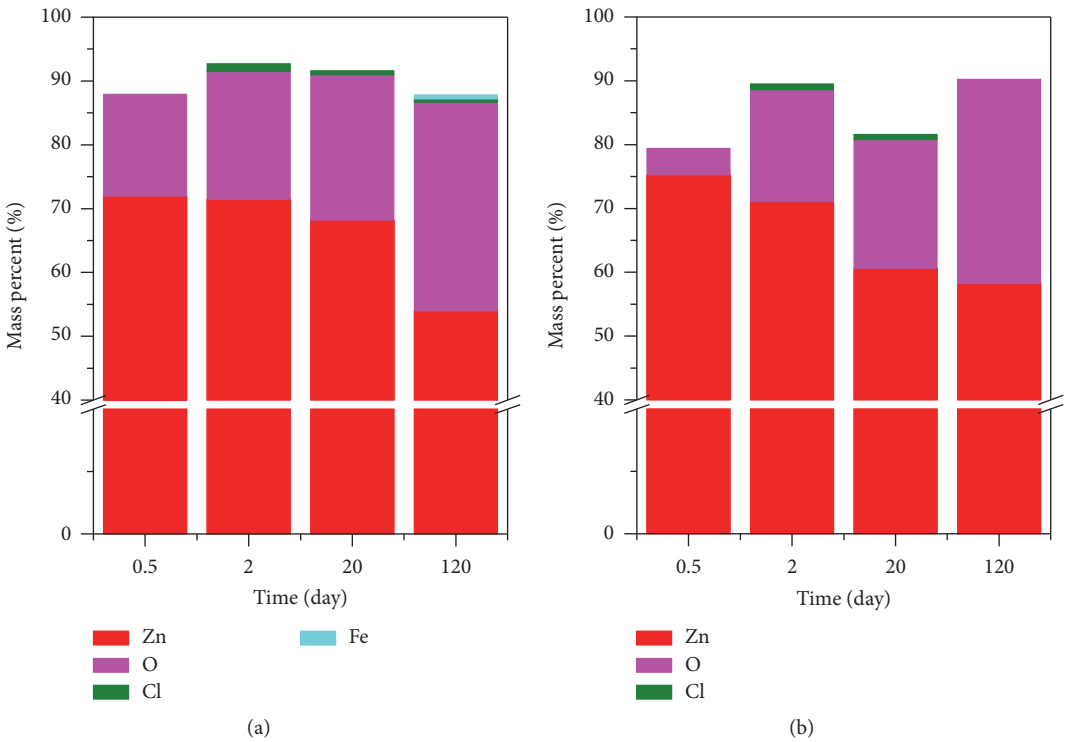

Figure 7: EDS mapping of PAni-ZRP (a) and PAni-ZnO-ZRP (b) at different immersion time.

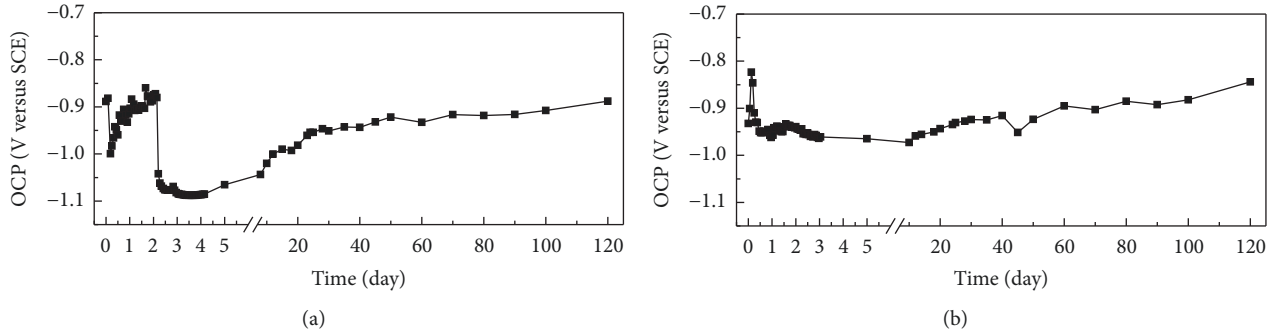

Figure 8: OCP changes over time for PAni-ZRP (a) and PAni-ZnO-ZRP (b).

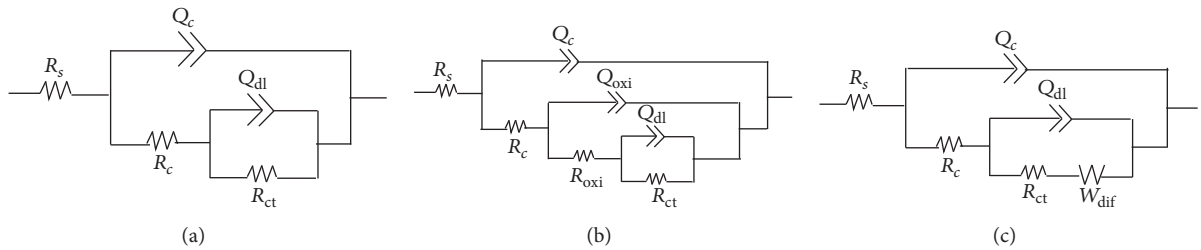

Figure 9: Electric equivalent circuits (EECs) models applied for EIS data fitting.

3.2. OCP and EIS Results and Discussion. OCP can be correlated to the anticorrosion performance stages of ZRP [2]. Three main periods were differentiated in the ZRP's lifetime after immersion in 3% NaCl solution: (a) the "activation" period, corrosion potential shifts to cathodic values; (b) in a second period, the electrode potential shifts to more anodic value and then reached the limit of CP; (c) at the third period, the corrosion potential is out of the CP range, and the coating provided barrier protection, depending on the formed zinc oxide products and coating morphology. The changes of OCP of PAni-ZRP and PAni-ZnO-ZRP coatings were detected after being immersed in 3.5 wt% NaCl solution from time to time. The OCP for steel 1018 was tested, being −860 mV versus SCE, which will be the limit potential of effective CP range. That is when OCP is more anodic than −860 mV, the cathodic protection provided by zinc particles disappears [31]. As shown in Figure 8, OCP increased slightly over time after 5 d immersion for the two coating systems. But the potential is still in OCP range, lower than −860 mV versus SCE which is the corrosion potential of bare steel used in this work.

Interestingly, the OCP presents a decreasing period in two different slopes at initial 5 d immersion except the sharp increase for PAni-ZRP, a faster slope and a slower slope, in agreement with the published work [2]. The higher slope is related to the activation of zinc particle and increasing area ration of Zn/Fe, and the slower decreasing slope was due to the increasing contact resistance between zinc particles. Later, the formation of zinc oxide products made the potential shift towards anodic value. Comparing these two coating systems, PAni-ZnO-ZRP coating system has more stable OCP than PAni-ZRP during the initial period. The sharp increase in OCP value for PAni-ZRP is because of the quick and accumulated formation of zinc oxide in coating interface.

The EIS results were fitted using equivalent electrical circuits (EECs) models to get valuable parameters related to coating evolution, as shown in Figure 9. These EEC models have been used in many published studies related to ZRPs [32–34]. R_s represents the electrolyte resistance; Q_c and R_c represent the constant phase element (CPE) and the resistance of the coating, respectively. Q_{oxi} and R_{oxi} represent the CPE and the resistance of the zinc oxide products, while Q_{dl} and R_{ct} represent the CPE of the double layer and the charge transfer resistance, respectively. W_{dif} represents the Warburg impedance. CPE elements are typically applied in the EIS fitting procedure to characterize the surface roughness at the interface [35] or to describe the frequency dependence of nonideal capacitive behavior [36]. The impedance of the Warburg diffusion element Z_w follows

$$Z_w = \sigma\left(1 - j\right)\omega^{-1/2}, \tag{4}$$

where σ is the Warburg coefficient, in units of $\Omega{\cdot}\mathrm{cm}^2{\cdot}\mathrm{s}^{-1/2}$. The CPE impedance is calculated using the following [35]:

$$Z\left(\mathrm{CPE}\right) = {Y_0}^{-1}\left(j\omega\right)^{-n}, \tag{5}$$

where Y_0 and n are the admittance and empirical exponents of CPE, respectively, j is the imaginary number, and ω is the angle frequency.

For both coatings, EIS Nyquist and bode phase diagrams are drawn in Figure 10 for different immersion time. Two

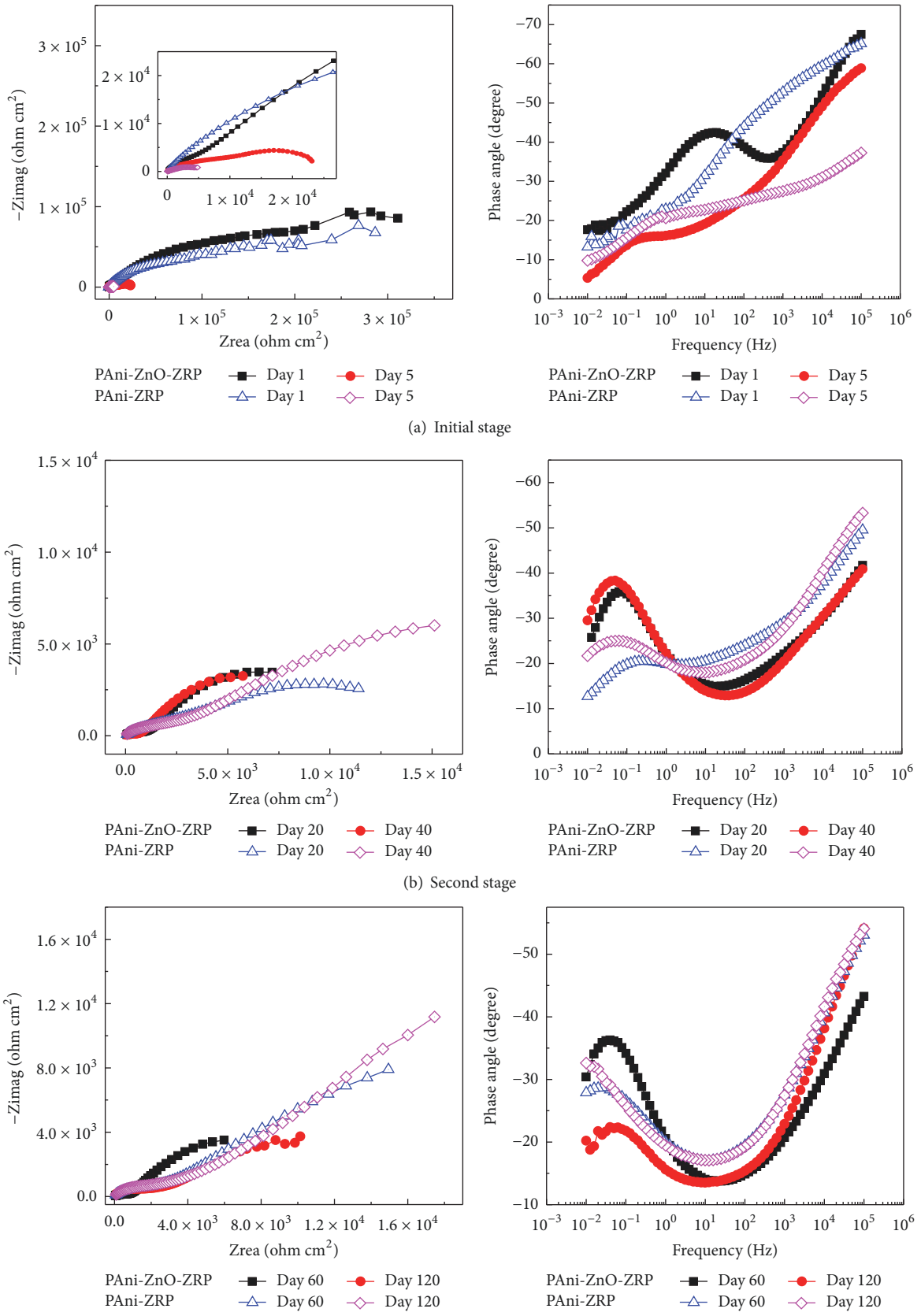

(a) Initial stage

(b) Second stage

(c) Third stage

Figure 10: EIS diagrams of PAni-ZRP and PAni-ZnO-ZRP at different stages.

Table 1: EIS fitting parameters of PAni-ZRP and PAni-ZnO-ZRP.

(a) Day 1 fitted using EEC shown in Figure 9(a)

Coating system	Y_c ($S{\cdot}s^n{\cdot}cm^{-2}$)	n_c	R_c ($\Omega{\cdot}cm^2$)	Y_{dl} ($S{\cdot}s^n{\cdot}cm^{-2}$)	n_{dl}	R_{ct} ($\Omega{\cdot}cm^2$)
PAni-ZRP	7.91×10^{-7}	0.62	8.74×10^4	7.84×10^{-6}	0.49	1.42×10^5
PAni-ZnO-ZRP	7.28×10^{-8}	0.74	1.07×10^5	1.09×10^{-6}	0.51	6.23×10^5

(b) Day 2 fitted using EEC shown in Figure 9(b)

Coating system	Y_c ($S{\cdot}s^n{\cdot}cm^{-2}$)	n_c	R_c ($\Omega{\cdot}cm^2$)	Y_{oxi} ($S{\cdot}s^n{\cdot}cm^{-2}$)	n_{oxi}	R_{oxi} ($\Omega{\cdot}cm^2$)	Y_{dl} ($S{\cdot}s^n{\cdot}cm^{-2}$)	n_{dl}	R_{ct} ($\Omega{\cdot}cm^2$)
PAni-ZRP	1.27×10^{-7}	0.77	1051	1.82×10^{-6}	0.43	1.56×10^5	1.34×10^{-5}	0.58	2.18×10^5
PAni-ZnO-ZRP	1.60×10^{-8}	0.75	7789	2.02×10^{-8}	0.48	4.29×10^5	4.57×10^{-5}	0.72	2.35×10^5

(c) Days 20, 60, and 120 fitted using EEC shown in Figure 9(c)

Time (day)	Y_c ($S{\cdot}s^n{\cdot}cm^{-2}$)	n_c	R_c ($\Omega{\cdot}cm^2$)	Y_{dl} ($S{\cdot}s^n{\cdot}cm^{-2}$)	n_{dl}	R_{ct} ($\Omega{\cdot}cm^2$)	σ_{dif} ($\Omega{\cdot}cm^2{\cdot}s^{-1/2}$)
PAni-ZRP							
Day 20	5.20×10^{-7}	0.71	152.6	6.41×10^{-5}	0.32	5441	12057
Day 60	2.78×10^{-6}	0.59	1679	2.66×10^{-6}	0.87	546.6	29798
Day 120	9.79×10^{-7}	0.65	1186	5.54×10^{-5}	0.35	5260	76884
PAni-ZnO-ZRP							
Day 20	3.69×10^{-6}	0.59	280	8.24×10^{-5}	0.39	878	10402
Day 60	5.70×10^{-6}	0.56	390.2	1.2×10^{-4}	0.42	895	10475
Day 120	4.41×10^{-7}	0.70	319.6	1.20×10^{-4}	0.20	6680	41375

time constants were observed in Nyquist diagram at the very beginning, fitted by EEC shown in Figure 9(a). Initially, coating PAni-ZnO-ZRP has larger R_c and R_{ct} than PAni-ZRP. This confirms the above immersion test results and SEM/EDS results. Pigments in the paint would induce pores, and nanostructure powders can fill in these pores to form uniform paint interface. When being immersed in corrosive environment, it would prevent the transportation of electrolyte and corrosive ions. Then quickly after 2 d, three time constants were observed and EEC shown in Figure 9(b) was used to fit the data. The semicircle at high frequencies was related to the organic coating matrix; the semicircle at medium frequencies was associated with the native zinc oxides, and the one at low frequencies was considered to represent the activation of the zinc particles when the electrolyte diffused through zinc oxide to reach the metallic zinc surface. At this stage, the coating PAni-ZnO-ZRP has larger R_c and R_{ct} than PAni-ZRP (Tables 1(a) and 1(b)), which explains the slower cathodic activation of zinc particles.

Over time, Nyquist diagram presents a circuit with two time constants combined with a small diffusion signal tail for both two coatings (Figure 10(b)), which was fitted using EEC shown in Figure 9(c). The diffusion signal appeared when the coating was covered by compact zinc oxide products. Notably, for PAni-ZnO-ZRP, the diffusion-controlled mechanisms' transport processes were recognized earlier in time (Day 8) than for PAni-ZRP (Day 10). Over 120 days (Figure 10(c)), the diffusion signal became more obvious, and the impedance increased. Comparing with PAni-ZRP, PAni-ZnO-ZRP has larger R_{ct} but smaller diffusion coefficient σ (Table 1(c)). It makes sense that, for PAni-ZRP, the assumption of zinc particles is faster than PAni-ZnO-ZRP confirmed from weight gain data in Figure 3(b). This formed more zinc corrosion products, which made the diffusion of oxygen much more difficult. The higher R_{ct} for PAni-ZnO-ZRP with slowly increasing R_c indicated the cathodic reaction of zinc particles slow and stable compared with PAni-ZnO.

For EIS results, resistance R_t at different frequencies were also extracted from bode modulus plots, which provided the visual ideas of coating interface properties, as discussed in many literatures [23, 24, 37]. For both two coating systems, three stages were obtained during 120 days of immersion (Figure 11), which agrees with OCP results. First, the activation stage was characterized by a dramatically decreasing coating resistance. Then it is the competition stage: characterized by an increasing Zn/Fe area ratio and increasing zinc contact resistance. After 60 d, the stable stage was obtained, with a slightly increasing resistance for PAni-ZnO-ZRP.

It is interesting that PAni-ZRP and PAni-ZnO-ZRP showed a very different performance during the initial few days (Figure 12). For PAni-ZRP, the first decreasing stage (0–Day 3) was combined by two repeat pattern substages. The first substage is from the beginning to 4 h, when the impedance dropped dramatically at all frequencies, related to activation of zinc particles. After 4 h till 15 h, the impedance increased due to the formation of zinc oxides. Then the impedance was kept stable till 51 h. This is considered as the first substage. Similarly, the impedance dropped drastically again followed by increasing impedance. From 57 h to 68 h, the impedance at frequencies lower than and including 10 Hz

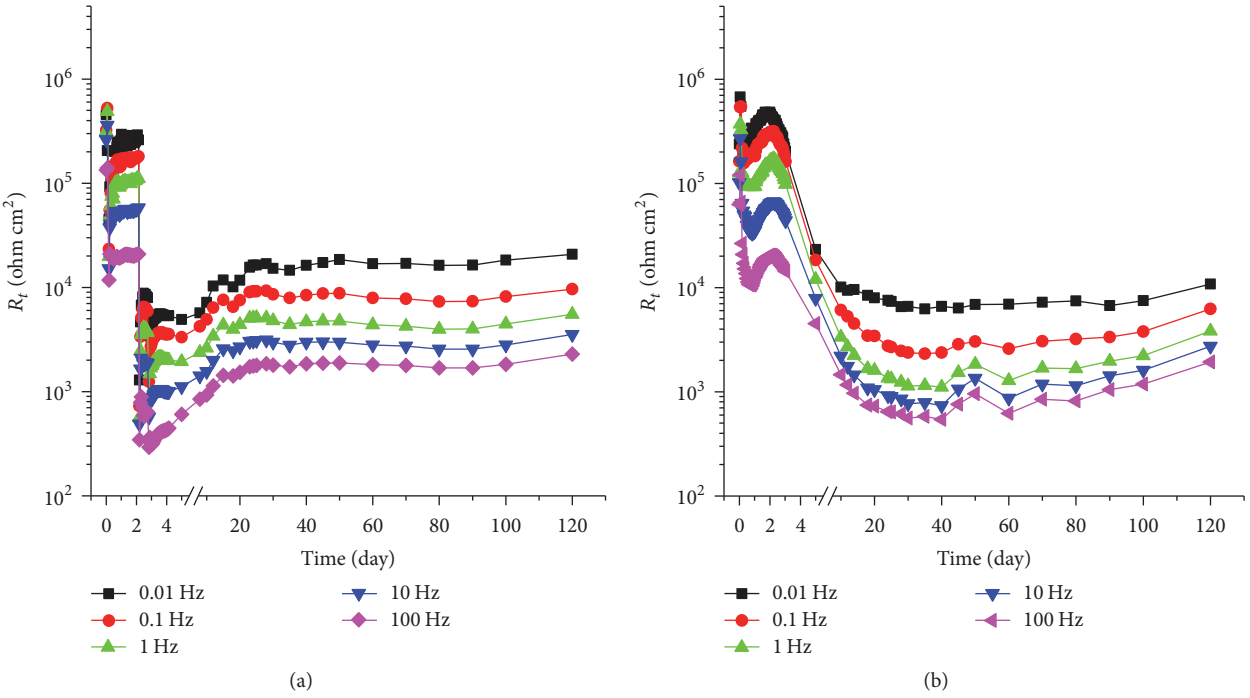

Figure 11: R_t value at various frequencies of PAni-ZRP (a) and PAni-ZnO-ZRP (b) over 120 days.

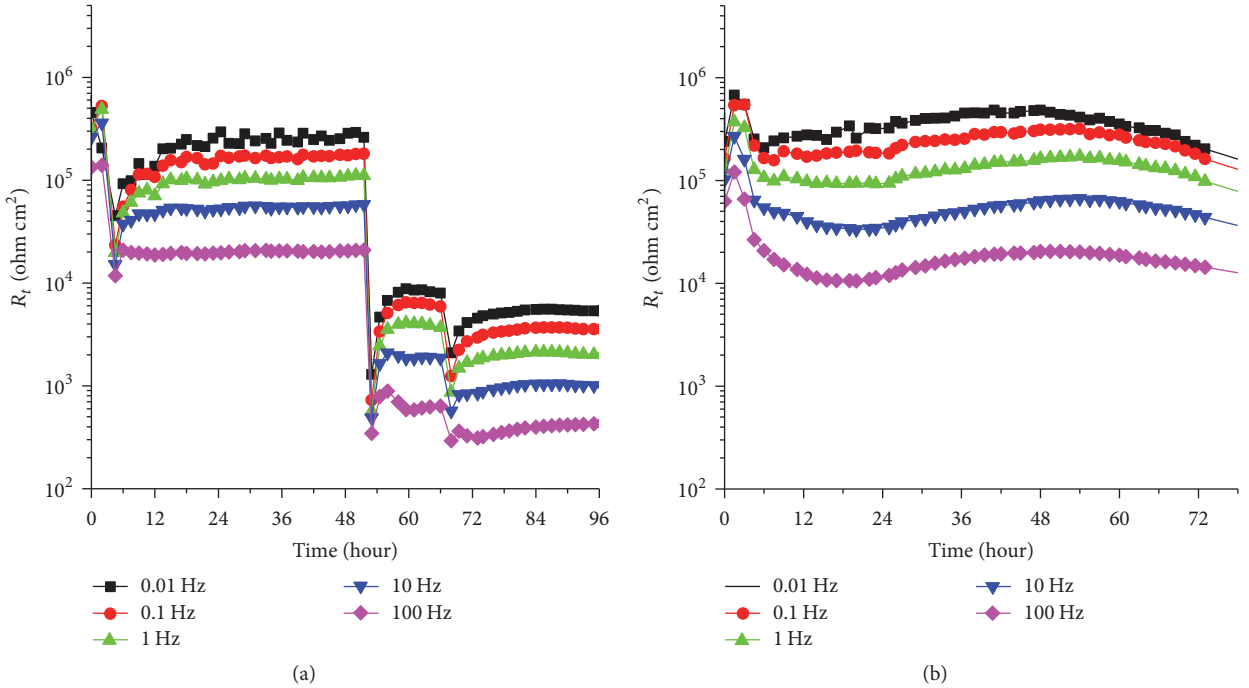

Figure 12: R_t value at various frequencies of PAni-ZRP (a) and PAni-ZnO-ZRP (b) at initial stage.

was stable, while the one at medium and high frequencies decreased and was then stable. This was considered as the second substage. These two substages were correlated to the activation of zinc particle in this coating interface, indicating that this process is not stable. In regard of PAni-ZnO-ZRP, three substages were observed: the fast decreasing, that is, first 4 hours of immersion. After 4 h to 25 h, the impedance decreased at a slower speed, while, after 25 hours, R_t slightly increased. It can also be seen that, for the initial stage, PAni-ZnO-ZRP has larger and more stable impedance compared with PAni-ZRP. This analysis indicated that the activation of zinc particles occurred much more slowly, which needs localized electrochemical technique to study.

3.3. SVET Results and Discussion

3.3.1. SVET Data Analysis Methodology. After SVET tests, the potential density was transferred to a current density, displayed in a three-dimensional (3D) map. The current mapping shows the spatial distribution of the current density as a function of the (x, y) position in the scan region on ZRPs. In addition, the contour map of the current densities is at the bottom of the 3D map. Considering the signal of current in the mapping, the negative current value is correlated with cathodic reaction, mainly occurring on steel surface, while the positive current values are correlated with anodic reaction, that occur at the zinc primer surface. SVET maps have been collected during 60 h of immersion for each sample. The total cathodic and anodic currents have been calculated at the scanning area to obtain the evolution of total current density over time, which has been applied in analysis of a massive amount of local ionic current distribution data maps [38]. The total anodic current density I_A and cathodic ionic current density I_C are calculated by integrating the current density i_z distribution across the scan area at different times, as shown in

$$I_C = \int_{x_{\min}}^{x_{\max}} \int_{y_{\min}}^{y_{\max}} \left[i_z\left(x; y\right) < 0\right] dx\, dy,$$
$$I_A = \int_{x_{\min}}^{x_{\max}} \int_{y_{\min}}^{y_{\max}} \left[i_z\left(x; y\right) > 0\right] dx\, dy, \quad (6)$$

where $x_{\max}$, $x_{\min}$, $y_{\max}$, and $y_{\min}$ are the coordinates of the scanning area. The evolutions of I_A and I_C have been calculated to compare these two coatings. It should be noticed that SVET is not always able to capture all of the localized currents [12]. It has been reported that SVET may not detect the activity occurring under the scanning plane if the galvanic interaction of the anodic and cathodic microsites occurs locally on the sample surface, and the circulation of cations and anions is concentrated essentially below the scan plane. The imbalance of anodic current and cathodic current has been discussed in [12, 33, 39]. To check this value, the total current was calculated following

$$I_{\text{int}} = I_A - I_C. \quad (7)$$

3.3.2. SVET Results and Discussion. The SVET current density maps together with contours for PAni-ZRP and PAni-ZnO-ZRP are presented in Figures 13 and 14, respectively, as a function of immersion time. The characteristic parameters I_{int}, I_A, I_C are shown in Figure 15. For PAni-ZRP, the anodic current was observed at zinc-rich primer, and cathodic current was detected on the steel surface after 6 h of immersion, indicating the activation of zinc cathodic protection. The current I_A, I_C increased fast during the following 24 h. Then the current decreased, and few anodic peaks were obtained on the ZRP surface. For PAni-ZnO-ZRP, anodic peaks were observed on ZRP surface at 6 h, same as PAni-ZRP, related to the activation of zinc particles. The current I_A, I_C slightly increased during initial few hours and became homogeneous after 8 h. However, this continuity disappeared after 24 h. Anodic bumps were obtained at the ZRP surface, especially at 60 h.

The characteristic parameters showed totally different behaviors for these two coatings. Four different stages were observed from Figure 15. The sacrificial cathodic reaction was activated with a quick increase of I_A and I_C till 30 h. This period is related to the cathodic reaction of zinc particles during activation stage. The formation of zinc oxide products made the current decrease, similar to these two coatings. For PAni-ZnO-ZRP, the third stage occurred during 30 h to 48 h, when I_A and I_C remained stable. Later, I_A and I_C increased again, which is not seen for PAni-ZRP. The sudden increase of current and anodic/cathodic peak obtained at 60 h may be related to the combination of PAni and ZnO, which may form a *p-n* junction, allowing the electrons to transport in only one direction in paint film [9]. Interestingly, PAni-ZnO-ZRP presents much smaller current value during 60 h of immersion compared with PAni-ZRP. This further proves that the addition of ZnO in PAni-ZRP makes the cathodic reaction of zinc particles slower. What is more, I_A and I_C in PAni-ZnO-ZRP decreased at earlier time than PAni-ZRP, after forming zinc oxide products in coating matrix, indicating that ZnO nanostructured particles improve coating barrier within reduction of passing routes used by electrolyte and corrosive ions.

As discussed above, three stages were observed by both OCP and EIS analysis. First, the activation stage was characterized by decreasing R_{ct}. Then the cathodic activation formed zinc oxide corrosion products in the coating matrix confirmed using SEM/EDS, which increased the Zn-to-Zn contact resistance. But Zn-to-Fe area ratio is also increased accompanied with the transportation of electrolyte and ions. This is considered as the competition stage characterized with a decreasing R_{ct} and an increasing diffusion resistance. After 60 d, the stable stage was attained, with a constant R_{ct} except Day 120 and an increasing diffusion resistance.

ZRP provides two protection mechanisms: barrier protection and CP. The barrier protection was demonstrated through immersion tests and surface morphologies. The SEM data show that the addition of nano-zinc oxide powders in coating matrix tends to produce less pores, uniform coating interface resulting in much larger initial R_c value from EIS fitting data. Besides, a diffusion-controlled process appeared earlier than observed for PAni-ZRP, which further proves

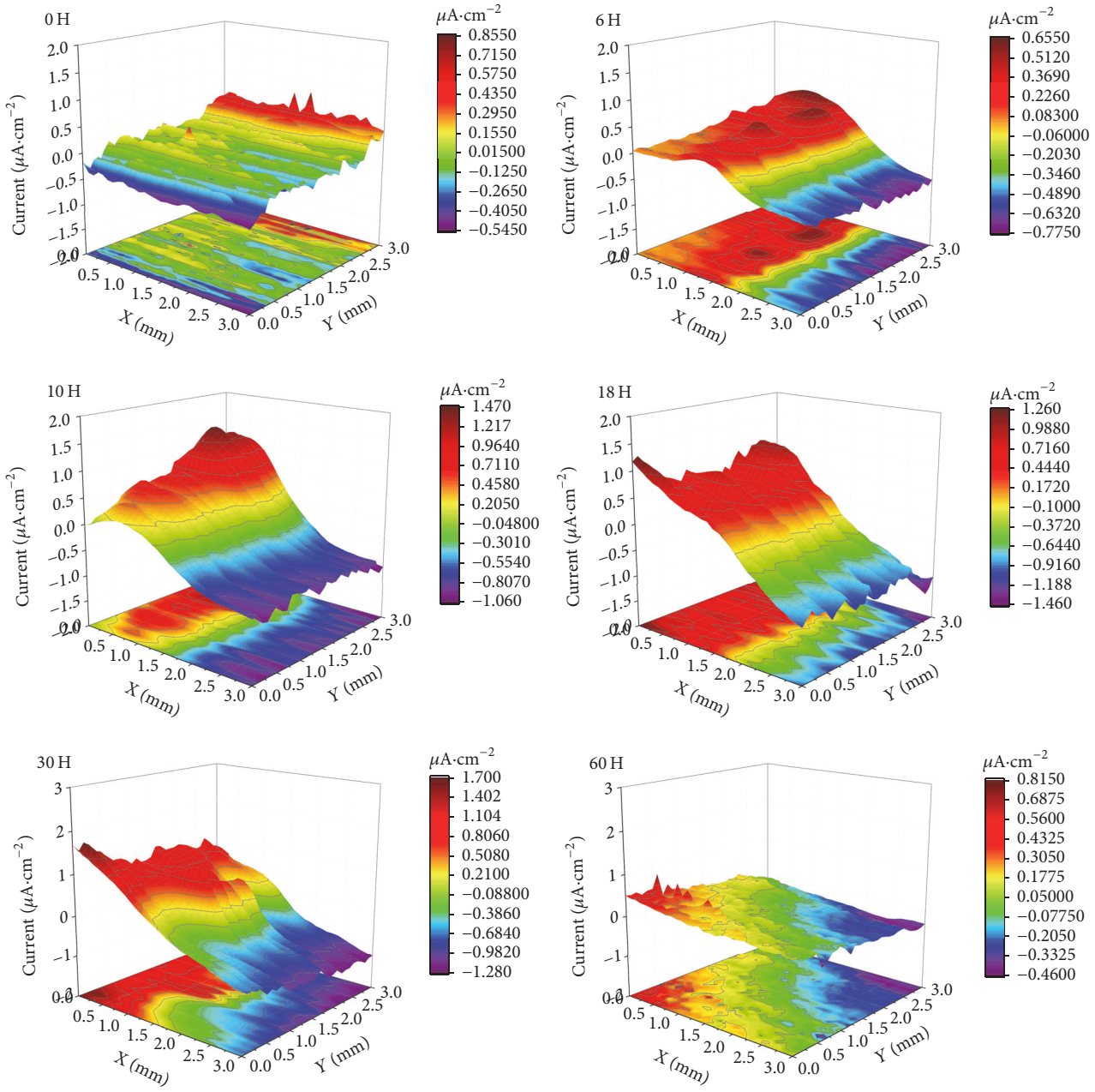

Figure 13: SVET current density maps for PAni-ZRP at different immersion time.

that the addition of ZnO improved the coating interface morphologies. In regard of CP effect, over 120 days of immersion, these two coatings are still in CP effective period through OCP test. Both EIS and SVET results show that the addition of nano-ZnO makes the cathodic activation of zinc slower and more stable. In our previous study, conductive polyaniline improved the Zn-to-Zn connection conduction of zinc-rich primer, referred to as percolation condition, which is critical for CP period. That is why over 120 days ZRP added with PAni are still in CP period. Considering the addition of nano-ZnO, it does not improve the percolation condition, but it filled in the pores caused by zinc and PAni particles which improves barrier performance. The uniform coating interface plus the good Zn-to-Zn connection helps to slow cathodic reaction of zinc, confirmed by EIS and SVET results. Another proposed mechanism is that ZnO and/or Zn^{2+} can interact with PAni and change its morphology into compact clusters on the metal/polymer interface which has been detected using localized electrochemical test SVET. This would facilitate formation of passive layer and hereby prevent

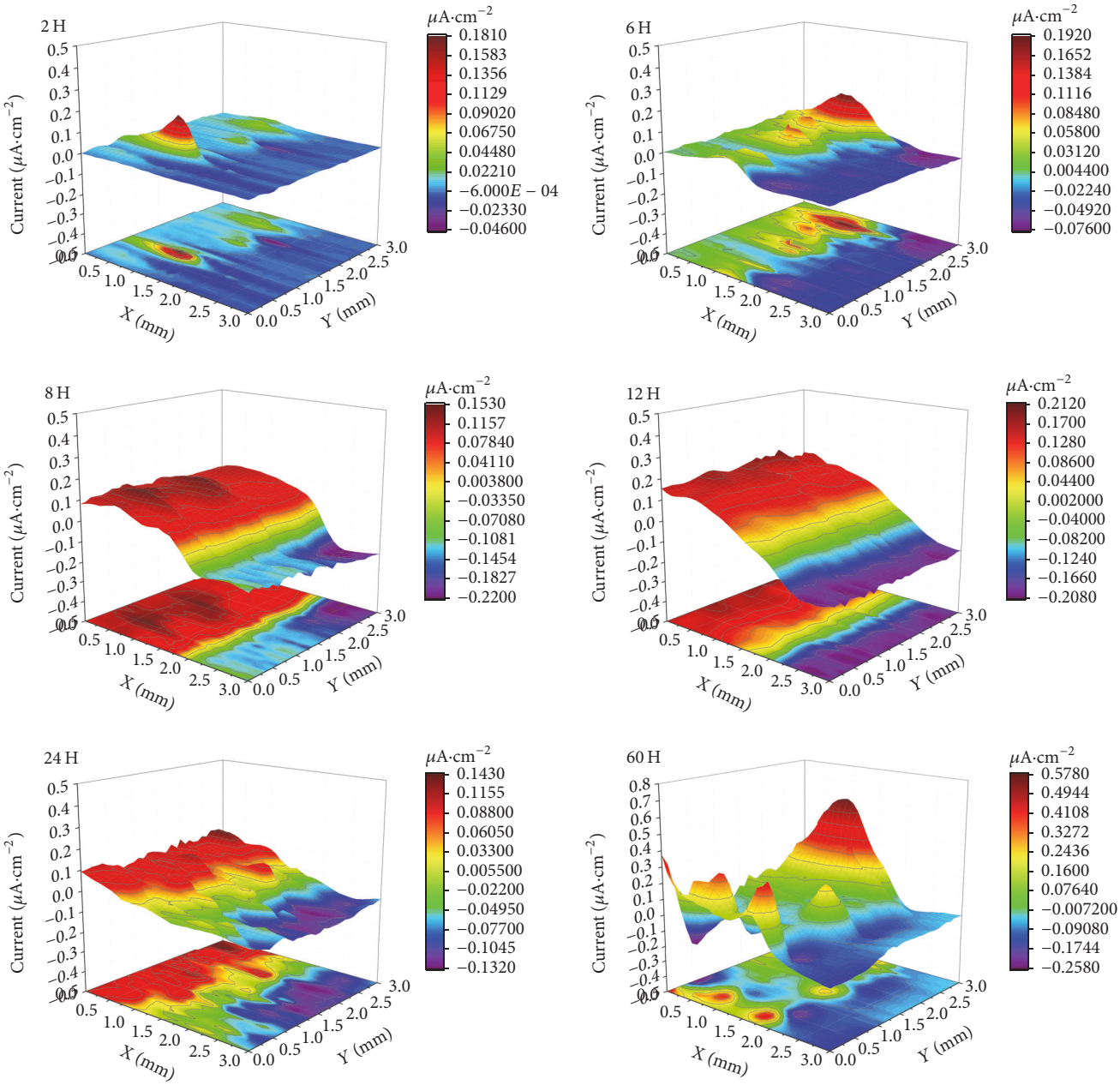

Figure 14: SVET current density maps for PAni-ZnO-ZRP at different immersion time.

further corrosion [12]. But this needs further continuing study.

4. Conclusion

Effect of zinc oxide nano particles on corrosion performance has been studied in conductive polyaniline containing zinc-rich primer, using Electrochemical Impedance Spectroscopy (EIS) and localized electrochemical Scanning Vibrating Electrode Technique (SVET). The results showed that the addition of nano-zinc oxide particles increased coating barrier performance. And nano-ZnO in coating matrix made the cathodic reaction of zinc more stable and slower, further to increase the effective cathodic protection period. The combination of PAni and ZnO was confirmed by SVET test.

For both two coating systems, three stages were obtained during 120 days of immersion. First, the activation stage was characterized by a decreasing charge transfer resistance R_{ct}. Then it is the competition stage: characterized by an increasing Zn/Fe area ratio and increasing zinc contact resistance. After 60 d, the stable stage was obtained, with a slightly increasing diffusion resistance.

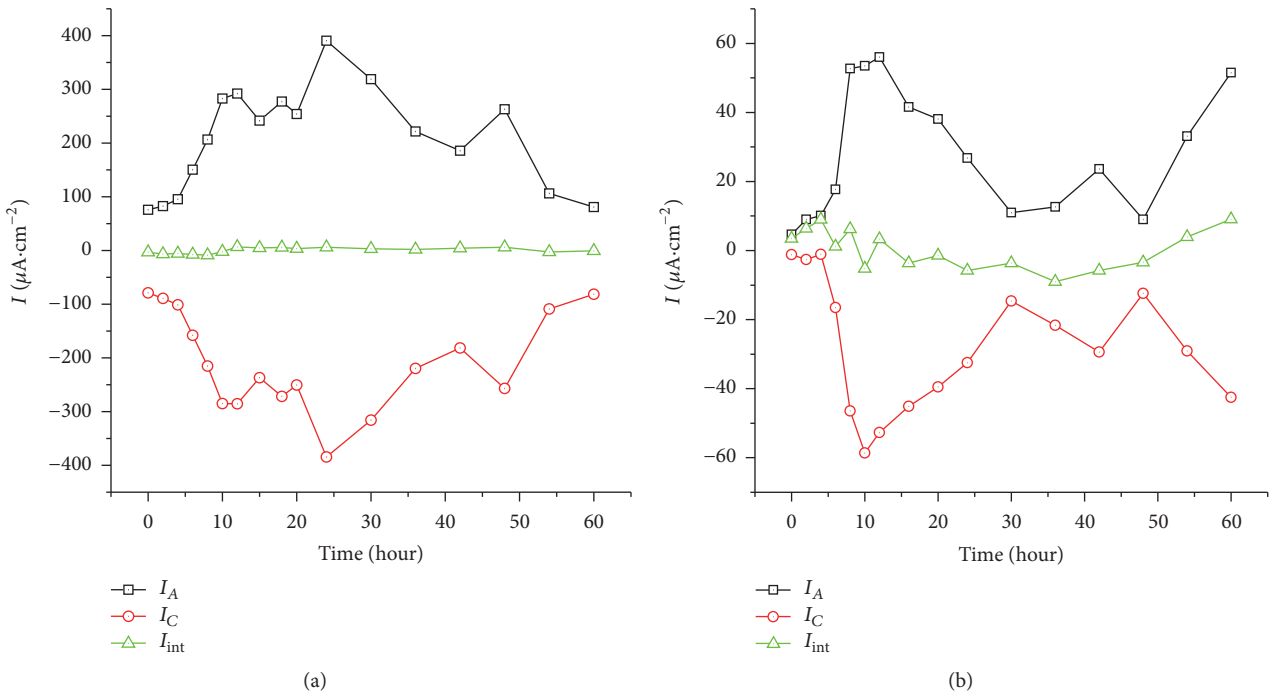

Figure 15: Characteristic parameters of SVET results above the scratched PAni-ZRP (a) and PAni-ZnO-ZRP (b) in 0.01 wt% NaCl solution.

Conflicts of Interest

The authors declare that there are no conflicts of interest regarding the publication of this paper.

References

[1] D. Pereira, J. D. Scantlebury, M. G. S. Ferreira, and M. E. Almeida, "The application of electrochemical measurements to the study and behaviour of zinc-rich coatings," *Corrosion Science*, vol. 30, no. 11, pp. 1135–1147, 1990.

[2] C. M. Abreu, M. Izquierdo, M. Keddam, X. R. Nóvoa, and H. Takenouti, "Electrochemical behaviour of zinc-rich epoxy paints in 3% NaCl solution," *Electrochimica Acta*, vol. 41, no. 15, pp. 2405–2415, 1996.

[3] H. Marchebois, M. Keddam, C. Savall, J. Bernard, and S. Touzain, "Zinc-rich powder coatings characterisation in artificial sea water EIS analysis of the galvanic action," *Electrochimica Acta*, vol. 49, no. 11, pp. 1719–1729, 2004.

[4] P. J. Kinlen, Y. Ding, and D. C. Silverman, "Corrosion protection of mild steel using sulfonic and phosphonic acid-doped polyanilines," *Corrosion*, vol. 58, no. 6, pp. 490–497, 2002.

[5] S. Bhadra, D. Khastgir, N. K. Singha, and J. H. Lee, "Progress in preparation, processing and applications of polyaniline," *Progress in Polymer Science*, vol. 34, no. 8, pp. 783–810, 2009.

[6] N. Y. Abu-Thabit and A. S. H. Makhlouf, "17 -Recent advances in polyaniline (PANI)-based organic coatings for corrosion protection," in *Handbook of Smart Coatings for Materials Protection*, A. S. H. Makhlouf, Ed., pp. 459–486, Woodhead Publishing, 2014.

[7] A. Meroufel, C. Deslouis, and S. Touzain, "Electrochemical and anticorrosion performances of zinc-rich and polyaniline powder coatings," *Electrochimica Acta*, vol. 53, no. 5, pp. 2331–2338, 2008.

[8] X. Li, D. Yang, and H. Castaneda, "Effect of different oxidation states of polyaniline on anticorrosion performances of modified zinc rich primer," in *CORROSION 2016*, NACE International, 2016.

[9] A. Mostafaei and F. Nasirpouri, "Epoxy/polyaniline-ZnO nanorods hybrid nanocomposite coatings: Synthesis, characterization and corrosion protection performance of conducting paints," *Progress in Organic Coatings*, vol. 77, no. 1, pp. 146–159, 2014.

[10] S. Sathiyanarayanan, S. S. Azim, and G. Venkatachari, "Corrosion protection of magnesium ZM 21 alloy with polyaniline-TiO2 composite containing coatings," *Progress in Organic Coatings*, vol. 59, no. 4, pp. 291–296, 2007.

[11] S. Sathiyanarayanan, S. S. Azim, and G. Venkatachari, "Preparation of polyaniline-Fe2O3 composite and its anticorrosion performance," *Synthetic Metals*, vol. 157, no. 18-20, pp. 751–757, 2007.

[12] A. Alvarez-Pampliega, S. V. Lamaka, M. G. Taryba et al., "Cut-edge corrosion study on painted aluminum rich metallic coated steel by scanning vibrating electrode and micro-potentiometric techniques," *Electrochimica Acta*, vol. 61, pp. 107–117, 2012.

[13] C. F. Glover, R. Subramanian, and G. Williams, "In-coating phenyl phosphonic acid as an etch-primer corrosion inhibitor system for hot dip galvanized steel," *Journal of The Electrochemical Society*, vol. 162, no. 9, pp. C433–C441, 2015.

[14] M. Kendig, F. Mansfeld, and S. Tsai, "Determination of the long term corrosion behavior of coated steel with A.C. impedance measurements," *Corrosion Science*, vol. 23, no. 4, pp. 317–329, 1983.

[15] J. Titz, G. H. Wagner, H. Spaehn, M. Ebert, K. Juettner, and W. J. Lorenz, "Characterization of organic coatings on

metal substrates by electrochemical impedance spectroscopy," *Corrosion*, vol. 46, no. 3, pp. 221–229, 1990.

[16] F. Mansfeld and C. H. Tsail, "Determination of coating deterioration with EIS I. Basic relationships," *Corrosion*, vol. 47, no. 12, pp. 958–963, 1991.

[17] C. H. Tsai and F. Mansfeld, "Determination of coating deterioration with EIS: part II. development of a method for field testing of protective coatings," *Corrosion*, vol. 49, no. 9, pp. 726–737, 1993.

[18] J. R. Macdonald, "Impedance spectroscopy: old problems and new developments," *Electrochimica Acta*, vol. 35, no. 10, pp. 1483–1492, 1990.

[19] C. G. Oliveira and M. G. S. Ferreira, "Ranking high-quality paint systems using EIS. Part I: Intact coatings," *Corrosion Science*, vol. 45, no. 1, pp. 123–138, 2003.

[20] C. G. Oliveira and M. G. S. Ferreira, "Ranking high-quality paint systems using EIS. Part II: Defective coatings," *Corrosion Science*, vol. 45, no. 1, pp. 139–147, 2003.

[21] X. M. Li, B. Faber, B. Minch, and H. Castaneda, "Analysis of soft coating corrosion performance on carbon steel using electrochemical impedance spectroscopy," *Corrosion*, vol. 70, no. 6, pp. 615–626, 2014.

[22] B. R. Hinderliter, S. G. Croll, D. E. Tallman, Q. Su, and G. P. Bierwagen, "Interpretation of EIS data from accelerated exposure of coated metals based on modeling of coating physical properties," *Electrochimica Acta*, vol. 51, no. 21, pp. 4505–4515, 2006.

[23] M. Mahdavian and M. M. Attar, "Another approach in analysis of paint coatings with EIS measurement: Phase angle at high frequencies," *Corrosion Science*, vol. 48, no. 12, pp. 4152–4157, 2006.

[24] Y. Zuo, R. Pang, W. Li, J. P. Xiong, and Y. M. Tang, "The evaluation of coating performance by the variations of phase angles in middle and high frequency domains of EIS," *Corrosion Science*, vol. 50, no. 12, pp. 3322–3328, 2008.

[25] E. Akbarinezhad, M. Bahremandi, H. R. Faridi, and F. Rezaei, "Another approach for ranking and evaluating organic paint coatings via electrochemical impedance spectroscopy," *Corrosion Science*, vol. 51, no. 2, pp. 356–363, 2009.

[26] X. Li and H. Castaneda, "Coating studies of buried pipe in soil by novel approach of electrochemical impedance spectroscopy at wide frequency domain," *Corrosion Engineering, Science and Technology*, vol. 50, no. 3, pp. 218–225, 2015.

[27] S. Li, "Monitoring corrosion using vibrational spectroscopic techniques," in *Intelligent Coatings for Corrosion Control*, pp. 673–701, Butterworth-Heinemann, Boston, Mass, USA, 2015.

[28] H. S. Isaacs, "The measurement of the galvanic corrosion of soldered copper using the scanning vibrating electrode technique," *Corrosion Science*, vol. 28, no. 6, pp. 547–558, 1988.

[29] A. International, *Standard Practice for Surface Wettability of Coatings, Substrates and Pigments by Advancing Contact Angle Measurement*, ASTM International, Conshohocken, Pa, USA, 2013.

[30] S. K. Dhoke and A. S. Khanna, "Study on electrochemical behavior of nano-ZnO modified alkyd-based waterborne coatings," *Journal of Applied Polymer Science*, vol. 113, no. 4, pp. 2232–2237, 2009.

[31] H. Marchebois, S. Joiret, C. Savall, J. Bernard, and S. Touzain, "Characterization of zinc-rich powder coatings by EIS and Raman spectroscopy," *Surface and Coatings Technology*, vol. 157, no. 2-3, pp. 151–161, 2002.

[32] J. S. Francisco, V. R. Capelossi, and I. V. Aoki, "Evaluation of a sulfursilane anticorrosive pretreatment on galvannealed steel compared to phosphate under a waterborne epoxy coating," *Electrochimica Acta*, vol. 124, pp. 128–136, 2014.

[33] A. G. Marques and A. M. Simões, "EIS and SVET assessment of corrosion resistance of thin Zn-55% Al-rich primers: Effect of immersion and of controlled deformation," *Electrochimica Acta*, vol. 148, pp. 153–163, 2014.

[34] S. Sathiyanarayanan, S. Syed Azim, and G. Venkatachari, "Corrosion protection coating containing polyaniline glass flake composite for steel," *Electrochimica Acta*, vol. 53, no. 5, pp. 2087–2094, 2008.

[35] C. H. Hsu and F. Mansfeld, "Concernng the conversion of the constant phase element parameter Y0 into a capacitance," *Corrosion*, vol. 57, no. 9, pp. 747-748, 2001.

[36] S. Skale, V. Doleček, and M. Slemnik, "Substitution of the constant phase element by Warburg impedance for protective coatings," *Corrosion Science*, vol. 49, no. 3, pp. 1045–1055, 2007.

[37] I. Sekine, K. Sakaguchi, and M. Yuasa, "Estimation and prediction of degradation of coating films by frequency at maximum phase angle," *Journal of Coatings Technology*, vol. 64, no. 810, pp. 45–49, 1992.

[38] R. M. Souto, Y. González-García, A. C. Bastos, and A. M. Simões, "Investigating corrosion processes in the micrometric range: A SVET study of the galvanic corrosion of zinc coupled with iron," *Corrosion Science*, vol. 49, no. 12, pp. 4568–4580, 2007.

[39] M. Yan, V. J. Gelling, B. R. Hinderliter, D. Battocchi, D. E. Tallman, and G. P. Bierwagen, "SVET method for characterizing anti-corrosion performance of metal-rich coatings," *Corrosion Science*, vol. 52, no. 8, pp. 2636–2642, 2010.